Dual-arm Object Manipulation by a Hybrid Controller with Kalman-Filter-based Inputs Fusion

Ching-Kai Chou, Wu-Te Yang, and Pei-Chun Lin

Abstract—**Grasping and manipulation of various objects by arms are essential robotic tasks. The dual-arm system in comparison with a single-arm system can grasp objects with larger sizes and shape variations owing to its high degree of task-space redundancy. We report on the development of a dual-arm manipulation strategy suitable for object holding and moving. The controller has master-slave structure. It hybridizes effects of the desired position trajectory (spatial relation) and the force interaction between the arm and the object (compliance), which includes maintaining adequate surface contact and normal force. The compensations of the position and force errors from the two controllers are fused in a Kalman filter to yield the control input for final motion correction. A dual-arm robot is built. The performance of the controller is experimentally evaluated, and the results conclude that the proposed control strategy can deal with position error, external force disturbance, and object weight variation.**

I. Introduction

For the last fifty years, industrial single-arm manipulators have been widely used in factory environments. In contrast, dual-arm systems are just emerging to be regarded as mainstream in robotics. The dual-arm system significantly increases object manipulability, and in the human environment there indeed exists many tasks requiring coordination between two arms. Examples include washing dishes, putting luggage in a compartment or trunk, stirring milk into coffee, etc. One of the benefits to using the dual-arm system is the capability of manipulating bigger objects owing to the intrinsic high degrees of freedom (DOF) for task-space redundancy. In addition, the closed kinematic chain formed by the dual-arm system and the object usually increases the object-grasping stability. Related works and applications can be found in a survey reported by Kragic et al. [1].

The force interaction between the two arms and the object is unavoidable in dual-arm manipulation. Force control is commonly used as the main control strategy, and surveys of the control algorithms can be found in research by Villani and De Schutter and Zeng and Hemami [2, 3]. In general, the force control can be categorized into two groups: indirect control and direct control. Indirect control accomplishes force control by means of motion control. One of most common control algorithms is the impedance control [4]. Thus, many researchers focus on the impedance behavior of the manipulator. The robot DLR uses virtual spatial springs, connected to the end-effectors in Cartesian space, and a coupling spring, connected to arms, to accomplish compliant behavior [5]. Researchers at KIST uses virtual spring-dampers connected to every joint and proposes a virtual dynamic model to reduce the impact during object manipulation [6].

Besides compliant behaviors, some researchers deal with planning and control. Based on work by Yul et al. [6], researchers at KIST transmit human motions to a humanoid robot with a motion-capture system to manipulate objects [7]. Researchers at JPL combine both vision and kinesthetic information to track both manipulator and object [8]. Shuji et al. use three tactile sensors equipped at the end-effector to detect the object surface orientation and keep the hand direction normal to the object surface in three dimensions [9].

Here, instead of directly focusing on a sophisticated manipulation task, we try to establish a straightforward control strategy that is inspired by a human manipulating a large object with his two arms. In addition to the algorithm, a dual-arm system is constructed for experimental evaluation. From a human perspective, three factors that affect the object manipulation after grasping are sense of space, sense of touch, and vision. The vision is important for grasping, but may be minor after the object is held. As a result, the former two factors are addressed in this paper. We investigate master-slave control strategy in three levels with different complexity. The right arm is equipped with a force/torque sensor (attached on the palm) and is considered as the slave side. The left arm without sensory feedback is considered the master side. The first-level controller is an open-loop position controller using spatial relation. Once the left arm is commanded to move, the right arm follows the left hand and maintains a certain spatial relation. Without using force information, the right arm can't adjust its force to hold the object when slippage happens. Thus, the second-level controller introduces compliance on the slave side by relating the force error to the velocity state. Two abilities are required for the palm to stably grasp the object: orienting the surface of the palm with that of the object and keeping the desired normal force between the palm and the object. The slave side with these two abilities can generate a fine touch of the object if the spatial movement is small. When the spatial movement is large, the force information on the arm is not sufficient to decouple the hand orientation or hand displacement. Thus, the motion of the master side is a priori for dual-arm spatial manipulation with the object. To remedy this limitation, we devised a third-level controller whose control input is created by fusing the position and control input and velocity control input of the first two levels with a Kalman filter infrastructure [10, 11]. Thus, the final controller is capable of

This work is supported by the National Science Council (NSC), Taiwan, under contract NSC 102-2221-E-002 -214 -MY3.

The authors are with the Department of Mechanical Engineering, National Taiwan University (NTU), No.1 Roosevelt Rd. Sec.4, Taipei 106, Taiwan. (Corresponding email: peichunlin@ntu.edu.tw)

simultaneously controlling both position and normal force. The slave side can regulate its pre-defined trajectory under external force disturbance by keeping its desired normal force. The proposed three-level control strategy is inspired by human dual-arm manipulation and provides a good connection between control law and the physical world.

Section II introduces the hardware of the dual-arm system, and Section III describes the control strategy. Section IV reports the experimental results, and Section V concludes the work.

II. HARDWARE OF THE DUAL-ARM SYSTEM

The dual-arm system consists of two PUMA-style arms. The arms are designed symmetrically, and the only difference lies in the sensory equipment, where the right arm has a 6-axis force/torque sensor (ATI). Table I lists the specifications of the arms. Fig. 1 shows the design concepts of the robot arm.

1. The rotation axes of the last three joints are designed to intersect at a point for easy inverse kinematics and for avoiding singularity.
2. The motor for the third DOF is installed close to the arm base, and its torque is transmitted to the joint via a pulley-and-belt system. This design reduces the arm inertia and provides the flexibility of further adjusting the torque-speed relation at the output.
3. Efforts are made to avoid geometrical offset, reducing the unwanted moment effect on the arm base.
4. A two-layer safety design is deployed to reduce the collision impact when the arm loses its control. The photo-isolators are used as the first-level electronic stoppers. The rubber dampers are used as the second-level mechanical stoppers.
5. The arm is constructed by thin aluminum plates and extrusions, which form a 3D structure to resist shear forces and torques.

The motors of the first three joints for translation motion use DC brushed motors, owing to the requirement of high torques. The motors of the last three joints for rotational motion use RC servomotors for their hardware and control simplicity. The effective rotational motion of the end-effector, composed of the last three joints, is similar to that of the human palm. Because the dual-arm system doesn't have a sophisticated hand or gripper, a flat surface is designed to act as the human palm, suitable for manipulating the object with parallel surfaces on the opposite sides. Fig. 2 shows the photo of the dual-arm system.

The dual-arm system uses a PC-based real-time platform as the computation center (PXI-8110, National Instruments), which has a 2.26-GHz Quad-Core CPU. Its interfacing with various I/O is done by using two PXI digital I/O boards that have 160 ports (PXI-7813R, NI). One D-I/O board is for general digital control, and the other board is for connecting a module convertor from R-series expansion chassis to C-series modules (NI 9151). The latter style is widely used on other robots in the lab, thus providing mechatronic compatibility. An analog input module (NI 9205) is used to connect the force/torque sensory data. The custom motor-drive module designed in our lab uses a switching amplifier (APEX SA57A). The incremental encoders are used for tracking

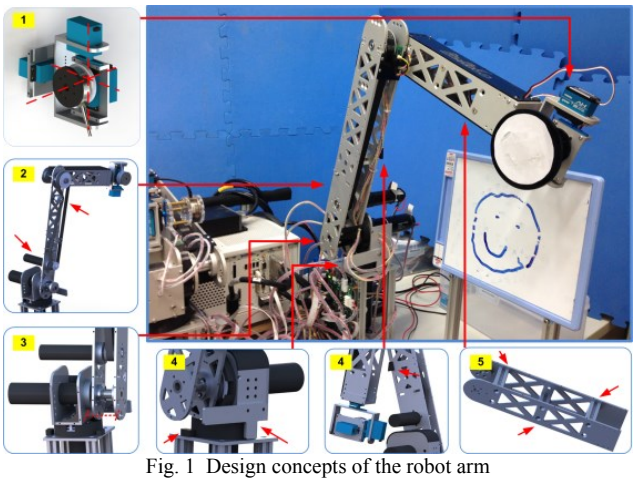

Fig. 1 Design concepts of the robot arm

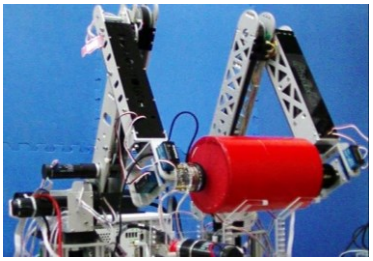
Fig. 2 Photo of the dual-arm system

TABLE 1 THE SPECIFICATIONS OF EACH ARM

Style	PUMA
DOFs	6
Arm length	1 m
Actuators	3 DC brushed motors for translational DOFs 3 servo motors for rotational DOFs
Weight	5 kg
Payload	1 kg

motor positions. The hall-effect sensors and photo interrupters are used for absolute positioning. The photo interrupters are also used for joint range limit protection.

III. DUAL-ARM MANIPULATION STRATEGY

A. Open-loop position control

Humans have a good sense of the relative positions of their arms. After an object is grasped, it can easily be manipulated, even when one's eyes are closed. This ability lies in the delicate force interaction and prescribed arm trajectories programmed by brain. The robot has better position control capability than humans, so it is intuitive to implement position control capability for dual-arm manipulation. When the object is grasped, the object length, L, using the right hand position, $\vec{P}_R$, and the left hand position, $\vec{P}_L$, can be computed

$$\left|\vec{P}_R - \vec{P}_L\right| = \mathrm{L} \tag{1}$$

The normal vector of the left palm, $\vec{n}_{L-palm}$, in Cartesian space is

$$\vec{n}_{L-palm} = {}^{0}_{T}R_L \times [0\ 0\ 1]^T \tag{2}$$

where ${}^{0}_{T}R_L$ is the rotation matrix from base frame to tool frame. In order to have the "object vector," defined as the vector connecting the center of two palms, to be consistent

(i.e., to simulate the object held in between), the desired right-hand position can be written as

$$\vec{p}_{R-desired} = \vec{P}_L + L \times \vec{n}_{L-palm} \quad (3)$$

where $\vec{p}_{R-desired}$ is equal to $\vec{P}_R$ at the beginning of manipulation. With the aim of manipulating the surface-parallel object, the desired right-hand orientation is identical to that of the left hand as

$$\vec{O}_{R\,desired} = \vec{O}_L \quad (4)$$

The overall process is depicted in Fig. 3.

Once the position and orientation of the left hand (i.e., the master side) is designed, the desired right-hand position and orientation can be quantitatively calculated. The position controller will ideally define the nominal motion of the two arms without considering the manipulation dynamics and disturbance and imperfection in the empirical system. The object may easily slip due to no monitoring of the normal force condition. Thus, the second-level controller is required, which aims to add some compliant behavior on the right hand (i.e., the slave side).

B. *Compliant control*

In order to stably grasp the object, the slave side should have fine contact with the object surface, and then it should provide certain normal force to the object. The controllers that satisfy the described two functions are hereafter referred to as "surface normal control" and "normal force control," respectively.

The concept of the surface normal control is mapping the torque to the object rotation by using PID compensation structure. The PID controller can be regarded as a second-order spring damper system. The process is described as follows. First, measure the 3-axis torques, τ, in the world frame, and normalize it by the normal force at contact

$$\tau_m = \tau / F_z \quad (5)$$

where F_z is the normal force in the tool frame. By setting the desired torque as zero, the PID controller maps torque to the palm rotational motion

$$\Delta\theta = \mathrm{k}(\tau_m - 0) + \mathrm{d}(\dot{\tau}_m - 0) \quad (6)$$

where k and d are PD parameters. Thus, when the torques measured by the sensor indicates that the palm doesn't contact with the surface well, the controller starts to adjust the palm orientation until the torques are eliminated. Fig. 4 shows the block diagram of the surface normal control.

The normal force control uses a similar principle, but the force/torque measurement and compensation motion generation are in different directions. The process is described as follows. First, measure the normal force in the tool frame and exclude the pull force to form the modified force f_m.

$$f_m = \begin{cases} 0, F_z \geq 0 \\ F_z, F_z < 0 \end{cases} \quad (7)$$

The desired normal force F_d and the modified force f_m form a virtual resultant force F_{sum}. The free-body diagram of the palm is shown in Fig. 5.

The virtual resultant force maps to the displacement using a PID controller

$$\Delta S = \mathrm{k}(F_{sum} - 0) + d(\dot{F}_{sum} - 0) \quad (8)$$

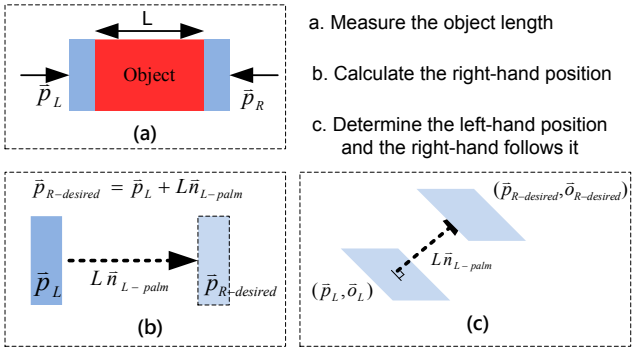

Fig. 3 Computation of the open-loop position control

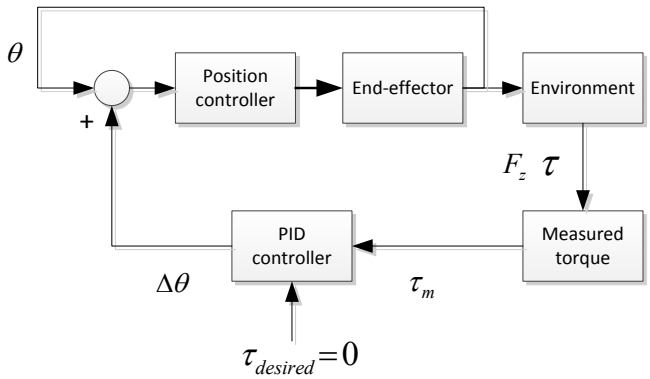

Fig. 4 Block diagram of the surface normal control

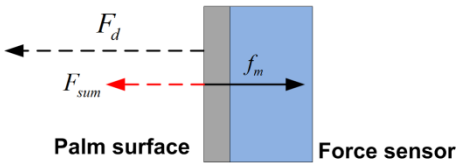

Fig. 5 The free-body diagram of the palm

The normal vector of the palm is chosen as the direction of the displacement

$$\Delta\vec{P} = \Delta S \times \vec{n}_{R-palm} \quad (9)$$

The block diagram of the normal force control is shown in Fig. 6.

If F_{sum} is greater than zero, it implies that F_d is greater than f_m. The controller pulls the palm along the normal direction until F_{sum} becomes zero. After that, f_m is equal to the desired normal force F_d. The palm can simultaneously touch the surface while maintaining desired normal contact force. Fig. 7 includes several snapshots extracted from one of the experiment runs. The photos shows that the human operator moves rightward and changes object orientation and the robot arm tracks the motion well.

By setting F_d equal to 5N, the slave side can cooperate with the human manipulating the object. Because the controller in the slave side doesn't incorporate the master side's spatial motion information as the open-loop controller does, the compliant controller can function only when the contact center has limited range of spatial motion. Reviewing the described two controllers, the open-loop position controller lacks compliant behavior, and the compliant controller doesn't incorporate spatial information. These two

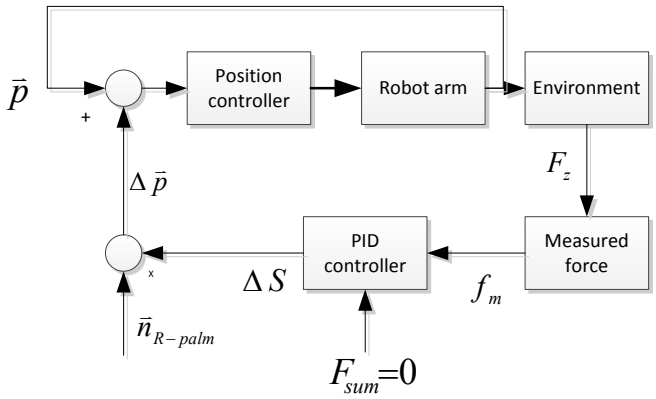

Fig. 6 Block diagram of the normal force control

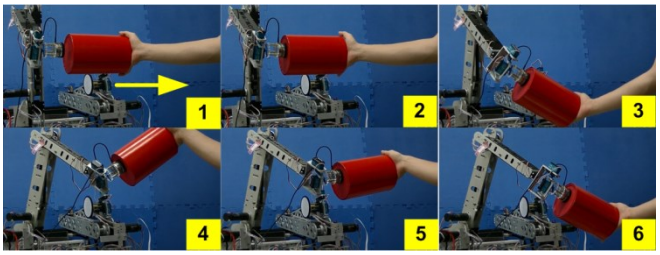

Fig. 7. The compliant motion of the robot arm to the human's spatial motion

controllers have complementary strengths that motivate us to fuse the compensation strategy together as the new hybrid controller.

C. *Hybrid control*

The hybrid control combines the compliant behavior and spatial relation. Fig. 8 shows the hybrid control scheme. The user determines the position and orientation of the left hand. By using the left-hand command and the object length, the open-loop control calculates the right-hand position and orientation. By using the measured force/torque, the compliant control calculates the change position and orientation. These two control inputs are fused by the Kalman filter. The fused position and orientation are used to control the slave side.

The control strategy is analogous to simple physics. As an object moves along the desired trajectory, external force acting on the object causes velocity change. The desired trajectory and velocity change form new measurements. The new measurements enter the Kalman filter to estimate better object states. In the hybrid control, the desired trajectory is analogous to the right-hand position and orientation, which is calculated by the open-loop position control. The velocity change is analogous to the change position and orientation, which is calculated by the compliant control. These two control inputs are treated as the measurements, and control outputs are regarded as the object states. Fig. 9 shows the block diagram of the hybrid control.

The positions of the estimated states by the Kalman filter is treated as the new control input to control the slave side. Because the control input of the hybrid controller comes from the control inputs of the other two controllers, the method of selecting the weight between spatial relation and compliant behavior is crucial. In ordinary Kalman filter operation, the

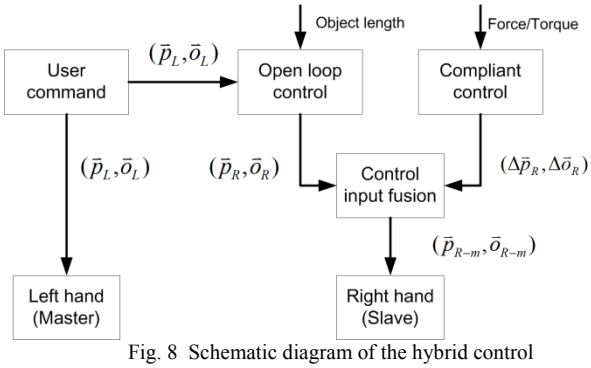

Fig. 8 Schematic diagram of the hybrid control

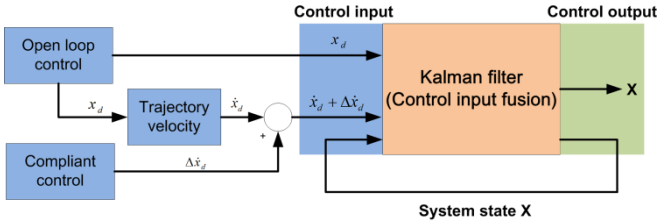

Fig. 9 Block diagram of the hybrid control

measurement noise covariance of individual sensors is usually empirically measured. If the covariance is larger than others, its measurement accuracy is considered less, and the optimization policy of the Kalman filter tends to weigh this measurement less. Following this analogy, if the weight of the compliant behavior increases, the trust level of the position control decreases. Without knowing the precise dynamic models of the system, it is extremely challenging to find the stochastic properties of the control inputs. Therefore, the weights of two inputs are treated equally. On the other hand, the process noise covariance determines the weights between measurements and system model. If magnitude of the process noise covariance is low, the Kalman filter tends to believe the system model more. Because the control inputs reside in position and velocity, the constant acceleration model is chosen as the system model. In this case, if the model covariance is considered small, the behavior of the control outputs tends to act as the constant acceleration motion, which yields smoother output. In the empirical implementation, six states, including three positions and three orientations (i.e., in Euler angles), are used to describe the position and orientation of the robot arm. Each state uses its own Kalman filter, so the weights for different motion states can be adjusted independently.

The slave side with the hybrid control can track the desired trajectory while keeping desired normal force. The next question lies in how to determine the ideal normal force. Normal force would provide enough static friction force to prevent slippage between the arm and the object. The friction force in general is equal to the shear force measured by the force/torque sensor

$$\mathrm{f} = \sqrt{{F_x}^2 + {F_y}^2} \tag{10}$$

Given the static friction coefficient, μ_s, the maximum static friction force can be expressed as

$$f_{static} = \mu_s F_z \tag{11}$$

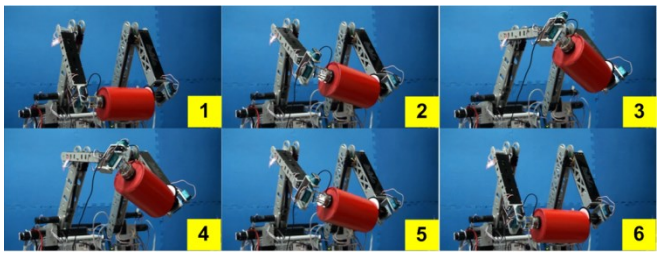

Fig. 10 Motion of the object generated by the dual-arm manipulation

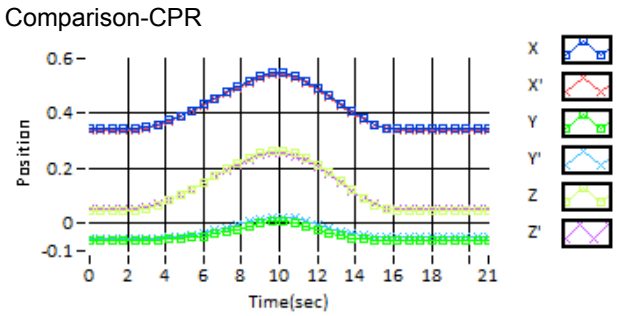

Fig. 11 State of the arm during dual-arm manipulation (the latter without and with single quotation—representing open-loop control and hybrid control)

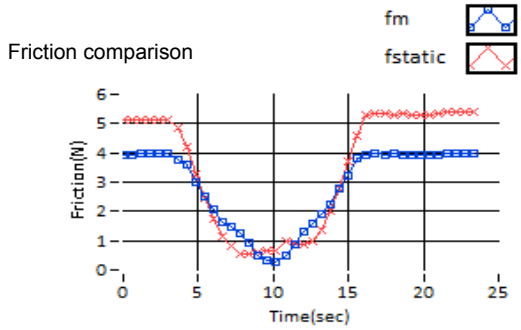

Fig. 12 The friction forces between the arm and the object while the arm is operated with the open-loop position control (blue represents measured friction and red represents maximum static friction)

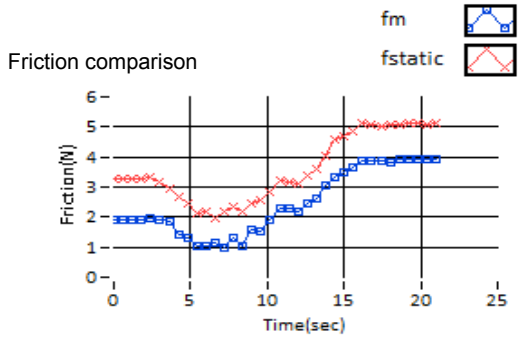

Fig. 13 The friction forces between the arm and the object while the arm is operated with the hybrid control (blue represents measured friction and red represents maximum static friction)

where F_z is the normal force measured in the tool frame. In order to avoid slippage, f_{static} must be greater than f. Thus, by setting a safety factor f_s, f_{static} and f have the relation

$$\mu_s F_z - f_m = f_s \tag{12}$$

The desired normal force can be expressed as

$$F_d = \frac{f_s + f_m}{\mu_s} \tag{13}$$

By setting the desired normal force as the described form, f_{static} is sufficient to withstand the weight of the object or external force disturbance.

IV. Experimental Result

The experiment results are reported in three subsections evaluating the performance of the controller described in Section IV. Subsection A discusses the comparison between the open-loop position control and the hybrid control by executing the same motion trajectory. Subsection B executes the same trajectory as Section A, but with external force disturbance during the process. Subsection C reports the experiment result when the arms hold a box still and extra weights (i.e., bottled waters) are added and taken out in sequence.

A. Object manipulation

The target is a cylinder (weight: 174g, height: 20cm, diameter: 13cm). The left hand is set to move 12cm in x direction and 10cm in z direction, and to rotate -35° in roll direction and 20° in yaw direction. The right hand follows to raise the object and put it back in the original position. Fig. 10 shows the snapshots of one of the experiment runs, and Fig. 11 plots the corresponding trajectories of the right hand, including those from both the open-loop position control and the hybrid control. It shows that hybrid control slightly adjusts the trajectory in comparison with the open-loop position control trajectory. Fig. 12 and 13 show the comparison between friction and maximum static friction in the open-loop position control and the hybrid control, respectively. In the former case, the plot shows that the friction is greater than the maximum static force, and this phenomenon causes slippage. In contrast, the hybrid control can keep the friction level below the maximum static friction.

B. Disturbance rejection

This experiment repeats the arm motion reported in subsection A, but with external force acting on the object. Figure 14 shows the snapshots of one of the experiment runs. With disturbance, the trajectory difference between the two controllers becomes clear, as shown in Fig. 15. The magnitude of the external disturbance force can be considered the same as the measured friction. The maximum impact force is about 12.5N. When the friction exceeds the maximum static friction, the maximum static friction quickly increases its magnitude. Figure 16 shows the status of the friction forces. When the impact force is removed, maximum static friction goes back to its proper value.

C. Manipulation with varying object weight

This experiment examines whether the dual-arm system can properly hold the object with in-situ weight varying. In order to clearly observe the friction change and to exclude the influence of moving dynamics, the dual arm is set to hold the box still. Fig. 14 shows the snapshots of one of the experiment runs. Fig. 15 clearly shows that the weights (bottled waters) are added at 2 and 5 seconds and taken away at 7.5 and 9.5 seconds, respectively. The maximum static friction is kept greater than the measured friction during the

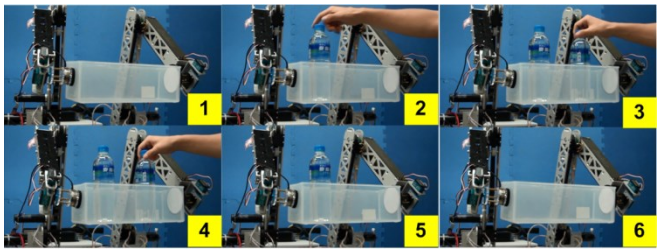

Fig. 14 Experiment with varying object weight

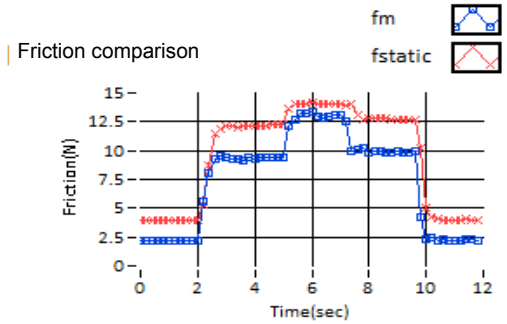

Fig. 15 The friction forces between the arm and the object while the arm is operated with the hybrid control in the varying object weight experiment (blue represents measured friction and red represents maximum static friction).

process, but the deviation is not constant. This phenomenon results from the fact that the hybrid control compromises between the spatial relation and the compliant behavior. When the weight of the box increases, the compliant controller tries to push the palm to touch the box. In contrast, the position controller tries to pull the palm back to its original desired position. The weight is adjustable by changing the covariance of both inputs.

V. Conclusion

In this paper, we report on a three-stage control strategy that is based on the master-slave structure. The first controller uses spatial relation. The user only has to determine the movement of the master side, and the slave side can follow it to manipulate objects in spatial motion. The second controller adds the compliant behavior to the slave side. The palm can touch the object surface while maintaining proper normal force. The third controller combines spatial relation and compliant behavior by using the Kalman filter. The effect of each behavior can be adjusted by the noise covariance measurement. With the help of the third controller, the slave side can adjust its predefined trajectory when external force disturbance exists and keep adequate friction force. Through experiments, we conclude that the third controller can deal with control error, external force disturbance, and weight variation.

References

[1] C. Smith, Y. Karayiannidis, L. Nalpantidis, X. Gratal, P. Qi, D. V. Dimarogonas, *et al.*, "Dual arm manipulation—A survey," *Robotics and Autonomous systems,* vol. 60, pp. 1340-1353, 2012.

[2] L. Villani and J. De Schutter, "Force control," *Springer handbook of robotics,* pp. 161-185, 2008.

[3] G. Zeng and A. Hemami, "An overview of robot force control," *Robotica,* vol. 15, pp. 473-482, 1997.

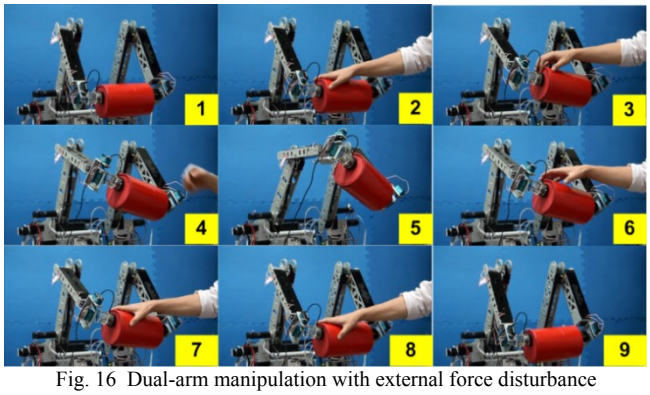

Fig. 16 Dual-arm manipulation with external force disturbance

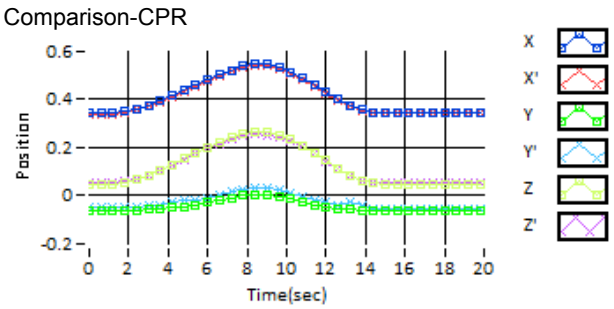

Fig. 17 State of the arm during dual-arm manipulation (the latter without and with single quotation—representing open-loop control and hybrid control under disturbance)

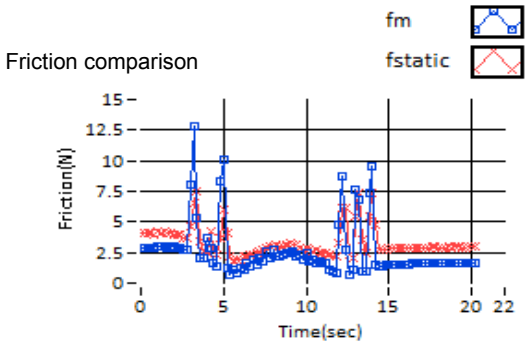

Fig. 18 The friction forces between the arm and the object while the arm is operated with the hybrid control and with external force disturbance (blue represents measured friction and red represents maximum static friction)

[4] N. Hogan, "Impedance Control: An Approach to Manipulation," in *American Control Conference, 1984*, 1984, pp. 304-313.

[5] T. Wimbock, C. Ott, and G. Hirzinger, "Impedance Behaviors for Two-handed Manipulation: Design and Experiments," in *Robotics and Automation, 2007 IEEE International Conference on*, 2007, pp. 4182-4189.

[6] S. Sung Yul, L. Jun won, and K. Chang Hwan, "Humanoid's dual arm object manipulation based on virtual dynamics model," in *Robotics and Automation (ICRA), 2012 IEEE International Conference on*, 2012, pp. 2599-2604.

[7] S. Y. Shin and C. H. Kim, "On-line human motion transition and control for humanoid upper body manipulation," in *Intelligent Robots and Systems (IROS), 2010 IEEE/RSJ International Conference on*, 2010, pp. 477-482.

[8] P. Hebert, N. Hudson, J. Ma, and J. W. Burdick, "Dual arm estimation for coordinated bimanual manipulation," in *Robotics and Automation (ICRA), 2013 IEEE International Conference on*, 2013, pp. 120-125.

[9] K. Suwanratchatamanee, M. Matsumoto, and S. Hashimoto, "Robotic tactile sensor system and applications," *Industrial Electronics, IEEE Transactions on,* vol. 57, pp. 1074-1087, 2010.

[10] G. Welch and G. Bishop, "An introduction to the Kalman filter," ed, 1995.

[11] R. E. Kalman, "A New Approach to Linear Filtering and Prediction Problems," *Transactions of the ASME-Journal of Basic Engineering,* vol. 82(Series D), pp. 35-45, 1960.